Supporting information

Inter-atomic synergistic Co-Zn diatomic catalyst for efficient H_2O_2 electrosynthesis in neutral and alkaline media.

Qiuyun Guo [a,b,c], Fantao Kong [*b], Xu Yu [b,c], Ningning Dai [d], Qin Li [b,c], Ping Wu [b], Han Tian [b], Kunming Song [a,b], Wenping Sun [e], Xiangzhi Cui [*a,b,c]

[a] School of Chemistry and Materials Science, Hangzhou Institute for Advanced Study, University of Chinese Academy of Sciences, Hangzhou 310024, PR China.

[b] State Key Lab of High Performance Ceramics and Superfine Microstructure, Shanghai Institute of Ceramics, Chinese Academy of Sciences, Shanghai 200050, PR China

[c] Center of Materials Science and Optoelectronics Engineering, University of Chinese Academy of Sciences, Beijing 100049, PR China.

[d] Shanghai Motor Vehicle Inspection Certification & Tech Innovation Center Co., Ltd.

[e] School of Materials Science and Engineering, State Key Laboratory of Clean Energy Utilization, Zhejiang University, Hangzhou, 310027 P. R. China.

*Email: cuixz@mail.sic.ac.cn (X. Cui).

1. Experimental Section

1.1 Materials

Melamine ($C_3H_6N_6$, 99%), Sulfur (S, 99%), Cobalt Phthalocyanine ($C_{32}H_{16}CoN_8$, 95%), Zinc Phthalocyanine ($C_{32}H_{16}N_8Zn$, 95%+), Potassium Sulfate (K_2SO_4, ≥99%), Cerium (IV) Sulfate ($Ce(SO_4)_2$, 99%+), Potassium hexacyanoferrate(III) ($K_3Fe(CN)_6$, 99%+) were purchased from Adamas Reagent Co. Ltd (Tansoole). Potassium Hydroxide (KOH, ≥85%), Hydrochloric acid (HCl), N,N-Dimethylformamide (C_3H_7NO, 99.8%) were purchased from Chinese medicine reagent. All chemicals were used as received without any further purification.

1.2 Materials preparation

Synthesis of S-C_3N_4

Firstly, a specified quantity of melamine was placed into a porcelain receptacle and calcined in a muffle furnace at 550 °C in air for 2 h (heating rate of 2.3 °C/min), after which it was cooled to room temperature in order to obtain the light yellow g-C_3N_4. Secondly, the g-C_3N_4 powder was subjected to ultrasonic protonation in a solution of 6 M HCl for one hour, followed by stirring for 4 h at room temperature. The acidic solution was then continuously washed with deionised water until the solution was neutral, after which it was dried in an oven to obtain the protonated layered g-C_3N_4. Subsequently, equal masses of protonated g-C_3N_4 and singlet sulphur were added to ball milling tank and ball milling for 4 h, with the objective of obtaining a well-mixed powder. Finally, a specific quantity of the combined powder was heated to 550 °C for 2 h under Ar atmosphere with a heating rate of 5 °C/min calcine to obtain S-doped C_3N_4.

Synthesis of Co/ZnPc-S-C_3N_4

Initially, 60 mg of S-C_3N_4, 3 mg of CoPc, and 2 mg of ZnPc were dispersed in 40 ml, 20 ml and 20 ml of DMF, respectively, and designated as Solution A, Solution B, and Solution C. Afterwards, solutions A, B, and C were sonicated for at least 30 min, respectively, so as to make the added materials well dispersed in the DMF. Subsequently, solution B and C were added to solution A and the mixture was

sonicated for at least 30 min. Finally, the sonicated mixture was stirred vigorously at room temperature for 48 hours and washed by centrifugation with ethanol and deionised water, and freeze-dried to obtain the Co-Zn heteronuclear diatomic catalysts Co/ZnPc-S-C_3N_4.

Synthesis of CoPc-S-C_3N_4、ZnPc-S-C_3N_4

Two control samples, including Co SAC CoPc-S-C_3N_4 and Zn SAC ZnPc-S-C_3N_4, were prepared by the same procedure, except that only 5 mg of CoPc was added in the preparation of CoPc-S-C_3N_4, while only 5 mg of ZnPc was added in the preparation of ZnPc-S-C_3N_4.

1.3 Materials characterization

Scanning electron microscope (SEM) images were obtained by Thermo Quattro S field emission environmental scanning electron microscope. Transmission electron microscopy (TEM) images were taken with a FEI Talos F200S field emission transmission electron microscope (200 kV). The atomic information and corresponding energy-dispersive X-ray spectrometer mapping (EDS-mapping) of Co/ZnPc-S-C3N4 were characterized using an FEI Themis Z transmission electron microscope operated at 200 kV and equipped with double spherical aberration (Cs) correctors. The powder X-ray diffraction (XRD) was recorded at 4^o min^{-1} on a Rigaku D/Max-2550 V X-ray diffractometer with a Cu Kα radiation target (40 KV, 40 mA). X-ray photoelectron spectroscopy (XPS) was collected using a Thermo Scientific K-Alpha XPS spectrometer. Raman spectra were performed using a LABRAM HR Evolution (785 nm). Ultraviolet-visible (UV-Vis) absorbance spectra were measured on a UV-1900i Spectrophotometer. The X-ray absorption spectroscopy (XAS) spectra were recorded in the transmission mode at the BL14W1 beamline of Shanghai Synchrotron Radiation Facility (SSRF).

1.4 O_2-TPD measurements

Weigh 100 mg of the sample in a reaction tube, warm up from room temperature to 290°C at 10°C min^{-1} for drying pretreatment, purge with He air flow (50 mL min^{-1}) for 1 h, cool down to 50°C, add 3% O_2/He mixture (50 mL min^{-1}) for 1 h to saturation, switch to He air flow (50 mL min^{-1}) and purge for 1 h

to remove the weakly adsorbed O_2 on the surface, and finally desorb under He atmosphere at a warming rate of 10°C min^{-1} to 290 °C. The surface was purged with He gas (50 mL min^{-1}) for 1 h to remove the weakly adsorbed O_2, and then finally desorbed at 290°C under He atmosphere with a heating rate of 10°C min^{-1}, and the desorbed gases were detected by TCD.

1.5 Electrochemical measurements

All the electrochemical measurements were performed at room temperature using a three-electrode system equipped with an electrochemical workstation. Among them, the selectivity of H_2O_2 was made on a CHI 760E electrochemical workstation, while all the test content of the H-type were performed with the biologic VSP-300 electrochemical workstation. A saturated Ag/AgCl electrode and a graphite rod were used as the reference and counter electrodes, respectively. A RRDE electrode with a glassy carbon electrode (0.2472 cm^2 area) and a platinum ring electrode (0.1856 cm^2 area) was used as the working electrode. The catalyst ink was prepared by dispersing 5 mg synthesized catalysts into 1950 μL of isopropanol and 50 μL 5.0 wt.% Nafion solution. Then the mixture was sonicated for at least 30 min to get homogeneous ink. Then aspirated 5μl drop of ink on the disk electrode and maked it dry naturally. Linear scanning voltammetry (LSV) measurements were conducted in an O_2-saturated 0.1M KOH or 0.1M K_2SO_4 electrolyte. The measured potentials versus Ag/AgCl were converted to the reversible hydrogen electrode (RHE) according to the following equation:

$$E_{RHE} = E_{Ag/AgCl} + 0.0591 \times pH + 0.1989\ V$$

The linear scanning voltammetry (LSV) tests were measured with an RRDE device, and the rotational speed and scanning rate were controlled to be 1600rpm and 10 mV s^{-1}, respectively. At the same time, a constant potential was applied to the Pt ring electrode as a means of monitoring the production of H_2O_2 on the disk electrode. The calculation of H_2O_2 selectivity and electron transfer (n) number follows the following two equations.

$$H_2O_2\ (\%) = 200 \times \frac{\frac{I_r}{N}}{|\ I_d\ | + \frac{I_r}{N}}$$

$$n = 4 \times \frac{|\ I_d\ |}{|\ I_d\ | + \frac{I_r}{N}}$$

Where I_d is the disk current and I_r is the ring current; and N is the collection efficiency of the ring with a value of 0.33, which was determined by the $[Fe(CN)_6]^{3-/4-}$ redox couple in 0.1 M KOH electrolyte with 10 mM $K_3Fe(CN)_6$ (Figure S26).

1.6 Measurement of electrochemical active surface area (ECSA)

The ECSA was determined using the double-layer capacitance (C_{dl}) method, which involves cyclic voltammetry (CV) measurements in the region of non-Faraday potentials. Specifically, CV curves were recorded in the region of 0.79 to 0.89 V vs Ag/AgCl at 10, 20, 40, 60, 80 and 100 mV s^{-1} scan rates. The double-layer capacitance (C_{dl}), which is linearly related to ECSA, was calculated by determining the slope value of $(j_a - j_c)/2$ at 0.24 V vs Ag/AgCl versus scan rate (where j_a is the anodic current density and j_c is the cathodic current density). The capacitance current density was also plotted versus scan rate to obtain C_{dl}.

1.7 Turnover frequency (TOF) calculation for H_2O_2 electrosynthesis

In our study, we used inductively coupled plasma mass spectrometry (ICP-MS) to estimate the active site densities for Co and Zn separately. We will calculate the TOF for the catalyst based on the number of Co and Zn active sites, following the relation:
The H_2O_2 current density (J_{H2O2}) was calculated by:

$$J_{H2O2} = J_{disk} \times FE$$

$$FE = \frac{S\%/100}{2 - S\%/100}$$

where J_{disk} is the disk current density, FE is the H_2O_2 faradaic efficiency, S% is the H_2O_2 selectivity. The kinetic current density (J_K) was then calculated by:

$$\frac{1}{J_K} = \frac{1}{J_{H2O2}} - \frac{1}{J_D}$$

where J_D is the diffusion-limited current density (3.025 mA cm-2 in 0.1 M KOH).

$$TOF = \frac{J_K}{2 \times F \times n_M}$$

Where F is the faraday constant (96,485 C mol^{-1}), n_M is the number of active sites.

1.8 Determination and quantitation of H_2O_2 using UV–vis

We used the $Ce(SO_4)_2$ method to detect the H_2O_2 concentration. Specifically, a certain amount of electrolyte from the electrolytic cell after $2e^-$-ORR was added to 5 mL of 0.4 mM $Ce(SO_4)_2$ solution. After mixing well, the absorption spectrum of the above solution was tested using a UV-visible spectrophotometer and the absorption intensity at 320 nm was recorded. A series of standard $Ce(SO_4)_2$ concentrations (0.04 mM, 0.08 mM, 0.12 mM, 0.16 mM, 0.20 mM, 0.24 mM, 0.28 mM, 0.32 mM, 0.36 mM, 0.40 mM) were measured in the same way as in the above mentioned tests to construct a concentration-absorbance curve to accurately quantify H_2O_2.

1.9 Measurement of H_2O_2 concentration

The operational yield of H_2O_2 was carried out in a two-compartment three-electrode H-cell system partitioned by an anion-exchange membrane. The working electrode was prepared by drip-casting Co/ZnPc-S-C_3N_4 ink onto 1.0 × 1.0 cm^2 carbon paper with a catalyst loading of 0.2 mg cm^{-2}. Ag/AgCl and carbon rods were used as reference and counter electrodes, respectively. Then, after reacting for 10 minutes at different potentials, the H_2O_2 yields tested at different potentials were quantified by the cerium sulphate titration method using the following reactions:

$$2Ce^{4+} + H_2O_2 \rightarrow 2Ce^{3+} + 2H^+ + O_2$$

where yellow-colored Ce^{4+} can be reduced by H_2O_2 to colorless Ce^{3+}, thus the yield of H_2O_2 ($^{\gamma_{H_2O_2}}$) can be calculated by the consumption of Ce^{4+} using the following equation:

$$C_{H_2O_2} = \frac{V_{Ce^{4+}} \times C_{Ce^{4+}_{before}} - \left(V_{Ce^{4+}} + V_{electrolyte}\right) \times C_{Ce^{4+}_{sfter}}}{2 \times V_{electrolyte}}$$

$$\gamma_{H_2O_2} = \frac{C_{H_2O_2} \times V}{t \times g}$$

where $V_{Ce^{4+}}$ is the volume of added $Ce(SO_4)_2$, $C_{Ce^{4+}_{before}}$ and $C_{Ce^{4+}_{sfter}}$ are the concentration of Ce^{4+} before and after reaction, respectively, $V_{electrolyte}$ is the volume of injected electrolyte after reaction, $C_{H_2O_2}$ is hydrogen peroxide concentration, V is the volume of electrolyte, t is reaction time, g is the mass of catalyst loading. The standard concentration-absorbance curve was obtained by linearly fitting the absorbance values at 320 nm for various known concentrations of Ce^{4+}. The faradaic efficiency (FE) value was calculated using the following equation:

$$\text{FE (\%)} = (2 \times \frac{C \times V \times F}{Q} \times 100\%)$$

where F is the Faraday constant (96485 C mol^{-1}); C is the concentration of generated H_2O_2; V is the volume of electrolyte (10 mL); and Q is the passed charge during the electrolysis.

2.0 Measurement of H_2O_2 concentration

Electrosynthesis of H_2O_2 via ORR was carried out using a flow cell in a two-compartment cell separated by a Nafion membrane. The formulated Co/ZnPc-S-C_3N_4 ink (2.5 mg mL^{-1}) was sprayed onto the surface of carbon paper (actual working area: 1 × 1 cm^2) with a catalyst loading of 0.125 mg cm^{-2} and form the cathode. Commercially available RuO_2 was used as the anode, while an Ag/AgCl electrode was used as the reference electrode. In the flow cell test, 1M KOH, 1M K_2SO_4 and 0.1M $HClO_4$ were used to test the H_2O_2 yield in different media. The electrolyte was circulated through peristaltic pumps at the cathode and anode. Meanwhile, O_2 was passed through the gas chamber connected to the cathode at a rate of 20 mL min^{-1}.

2.1 Theoretical calculation

All density functional theory (DFT) calculations in this study were conducted using the Vienna Ab initio Simulation Package (VASP) within the framework of the generalized gradient approximation (GGA) employing the Perdew-Burke-Ernzerhof (PBE) functional[1, 2]. Ionic cores were described using the projected augmented wave

(PAW) potentials, while valence electrons were treated with a plane-wave basis set and a kinetic energy cutoff of 450 eV. Partial occupancies of Kohn−Sham orbitals were included using Gaussian smearing with a width of 0.05 eV. Geometric and lattice optimizations were performed with a Brillouin zone integration using 1x1x1 *Γ*-centered *k*-point sampling[3]. The convergence criteria for self-consistent calculations were set to an energy threshold of 10^{-5} eV, and equilibrium geometries were optimized until the maximum atomic force was below 0.02 eV/Å. To minimize interactions between periodic images, a 15 Å vacuum layer was introduced. Weak interactions were accounted for using the DFT+D_3 method with Grimme's empirical correction. Spin polarization was incorporated to describe the magnetic system. Post-processing of input and output data, including charge difference analysis, was conducted using Vaspkit. Bader charge[4] analysis was also performed. To address the strong correlation effects of transition metals, structural optimizations and electronic structure calculations employed the spin-dependent GGA+U approach, with effective Ueff parameters were 3.32 eV for Co atom[5] and 6.0 eV for Zn atom[6].

2. Supporting figures

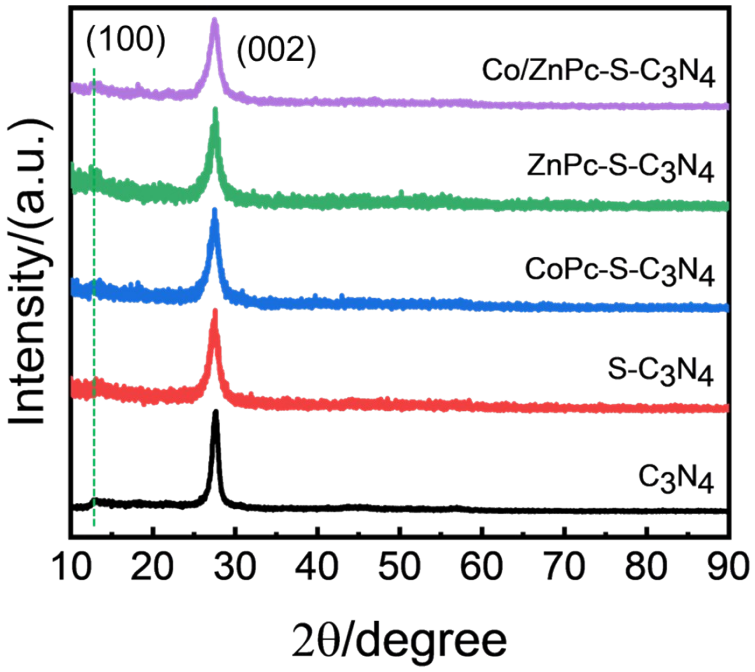

Figure S1. XRD patterns of Co/ZnPc-S-C_3N_4, CoPc-S-C_3N_4, ZnPc-S-C_3N_4, S-C_3N_4 and C_3N_4, respectively.

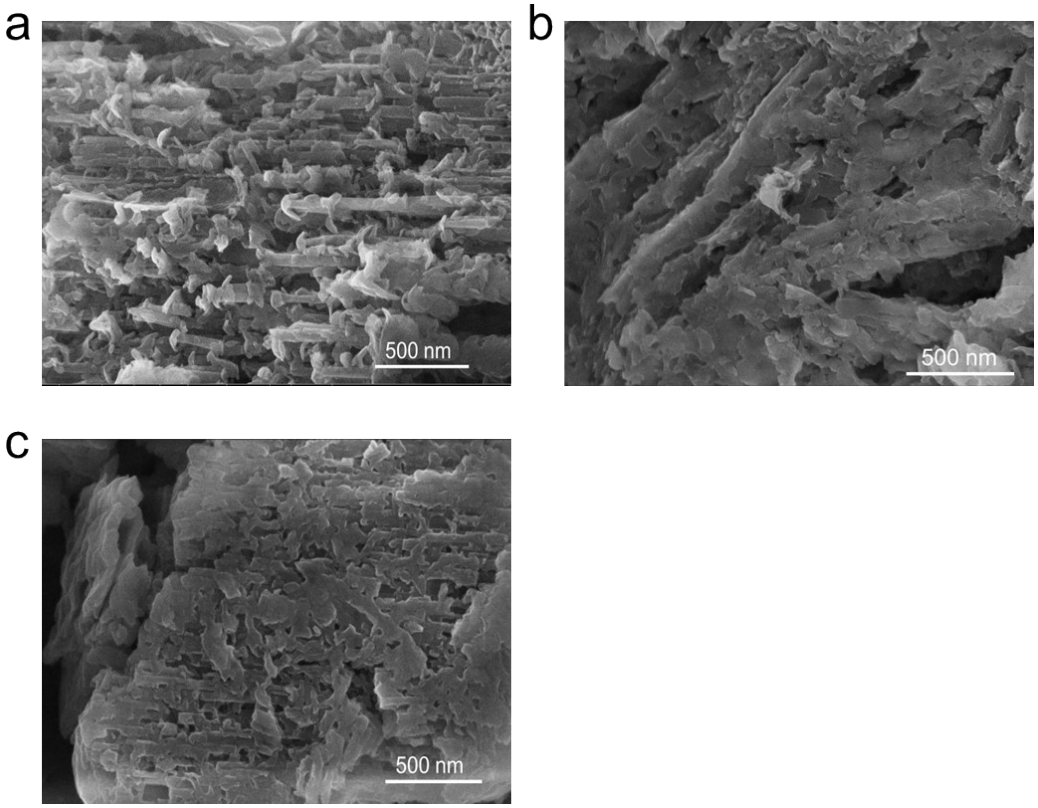

Figure S2. SEM images of (a) C_3N_4, (b) S-C_3N_4, (c) Co/ZnPc-S-C_3N_4.

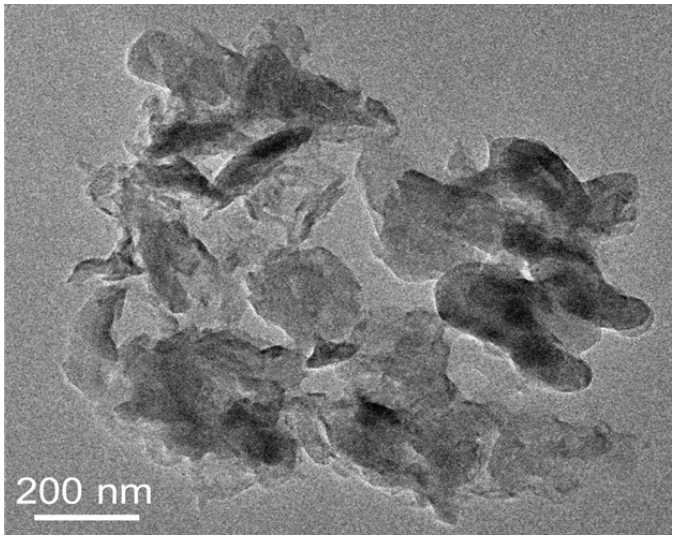

Figure S3. SEM image of Co/ZnPc-S-C_3N_4.

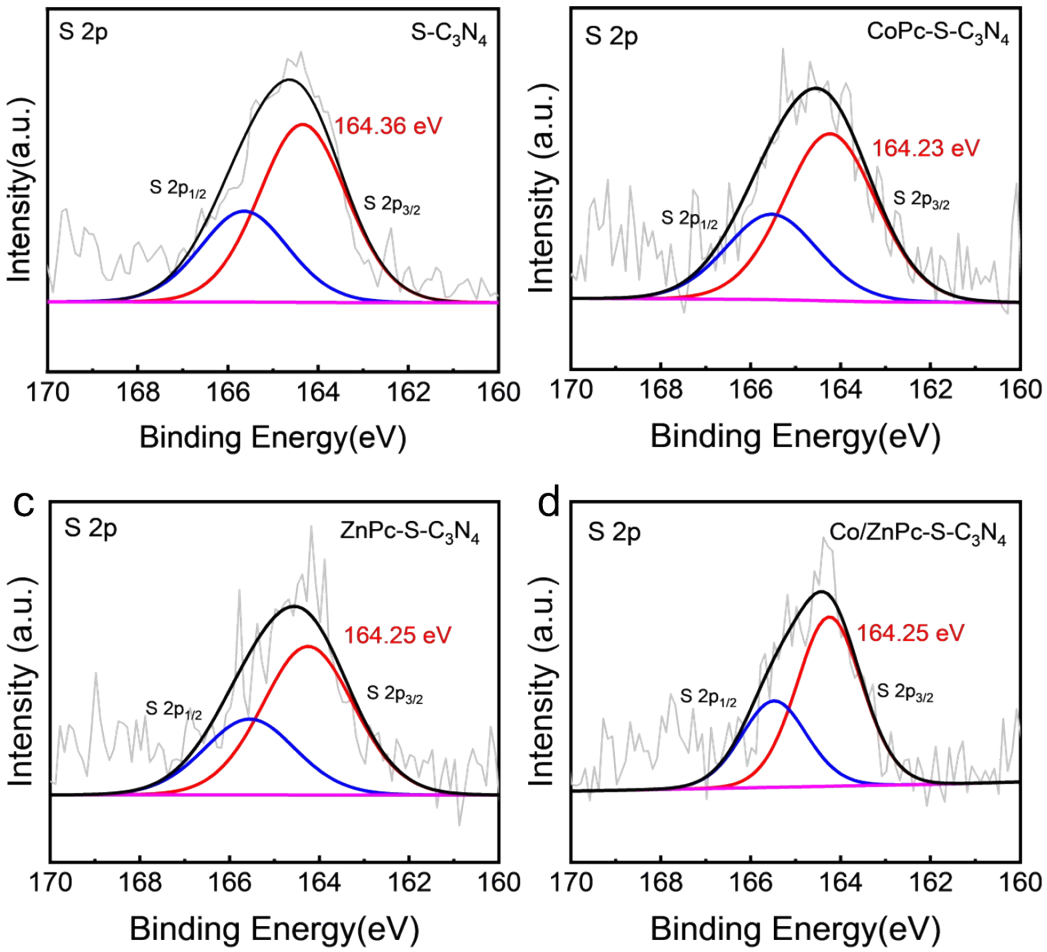

Figure S4. S 2p XPS spectra of (a) S-C_3N_4; (b) CoPc-S-C_3N_4; (c) ZnPc-S-C_3N_4 and (d) Co/ZnPc-S-C_3N_4.

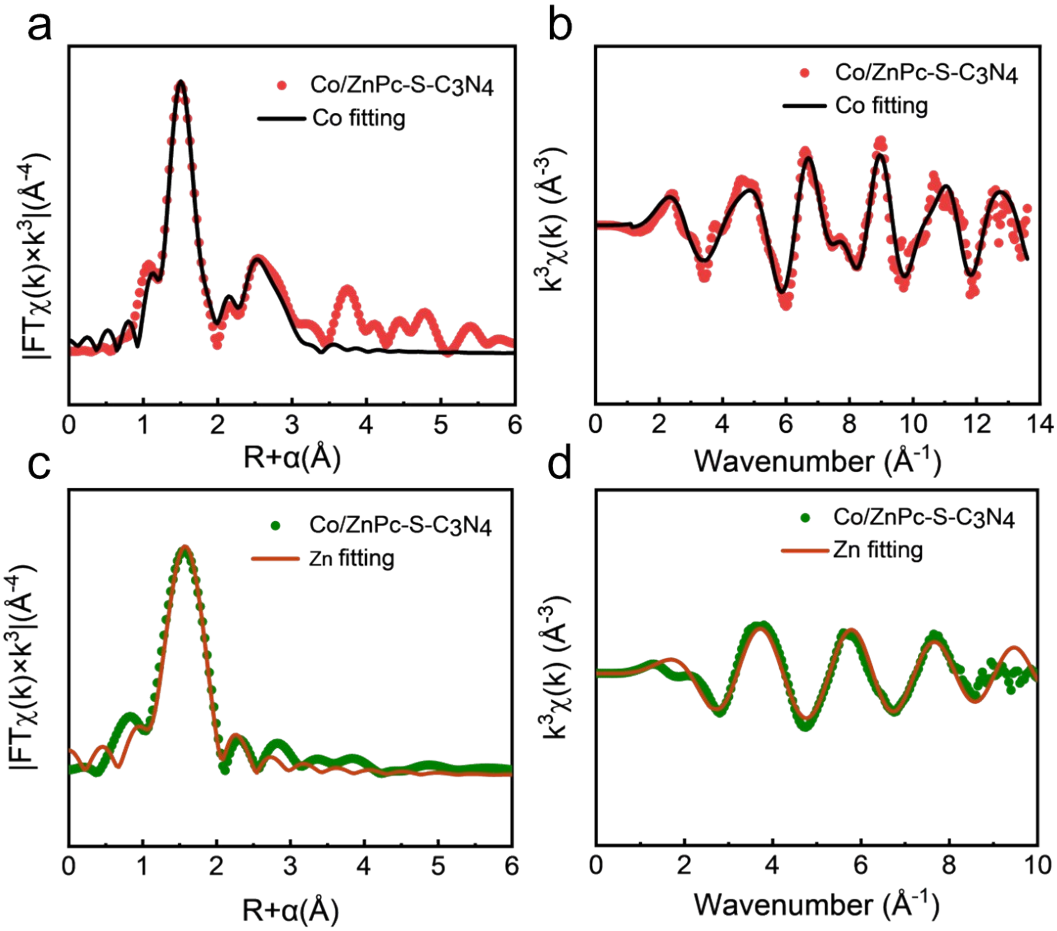

Figure S5. Fourier transform EXAFS spectra (a) and the corresponding curve-fitting results (c) of Co/ZnPc-S-C_3N_4. (b) Co and (d) Zn K-edge EXAFS fit about k^3-weighted k-space for Co/ZnPc-S-C_3N_4.

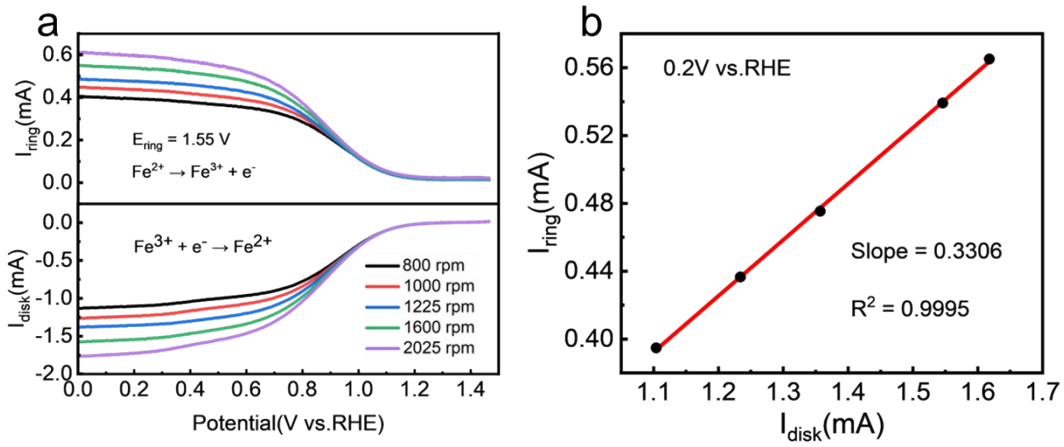

Figure S6. RRDE collection efficiency calibration (a) Linear sweep voltammetry curves recorded on bare glassy carbon rotation disk electrode with Pt ring in an N_2 saturated electrolyte with 0.1 M KOH+10 mM $K_3Fe(CN)_6$. Sweep rates: 20 mV/s, E_{ring} = 1.55 V vs.RHE. (b) Linear fits of diffusion-limited current densities recorded at different rotational speeds on ring and disk electrodes. The experimentally determined apparent collection efficiency (N) of 0.33 is close to the theoretical value of 0.37.

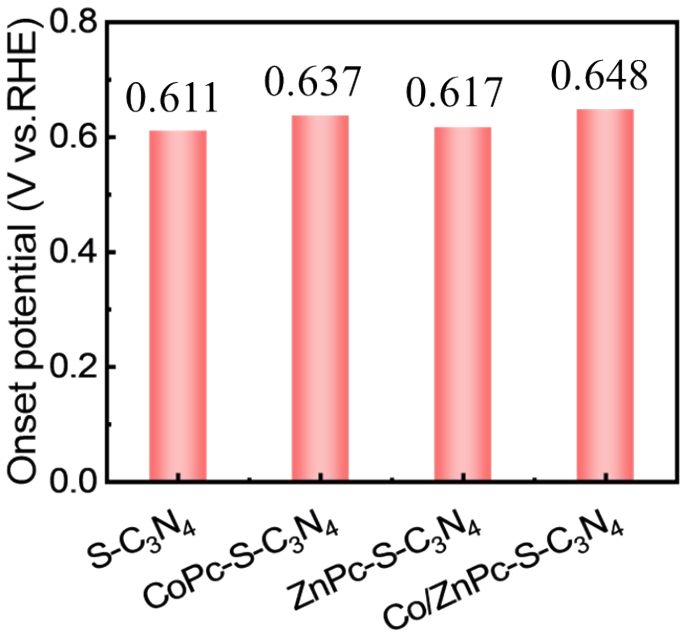

Figure S7. Histograms of the onset potential at current density of 1 mA cm^{-2} in 0.1M KOH electrolyte.

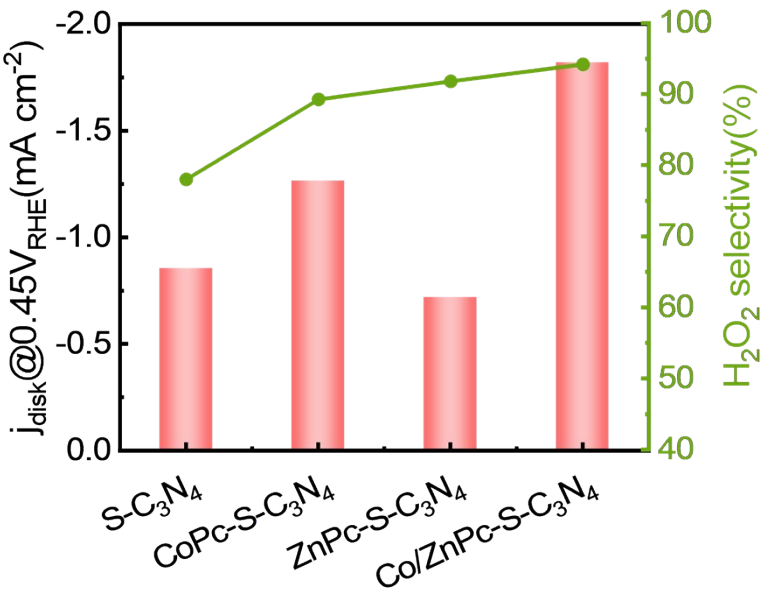

Figure S8. Relationship between current density, H_2O_2 selectivity and loaded MPc in 0.1 M KOH electrolyte.

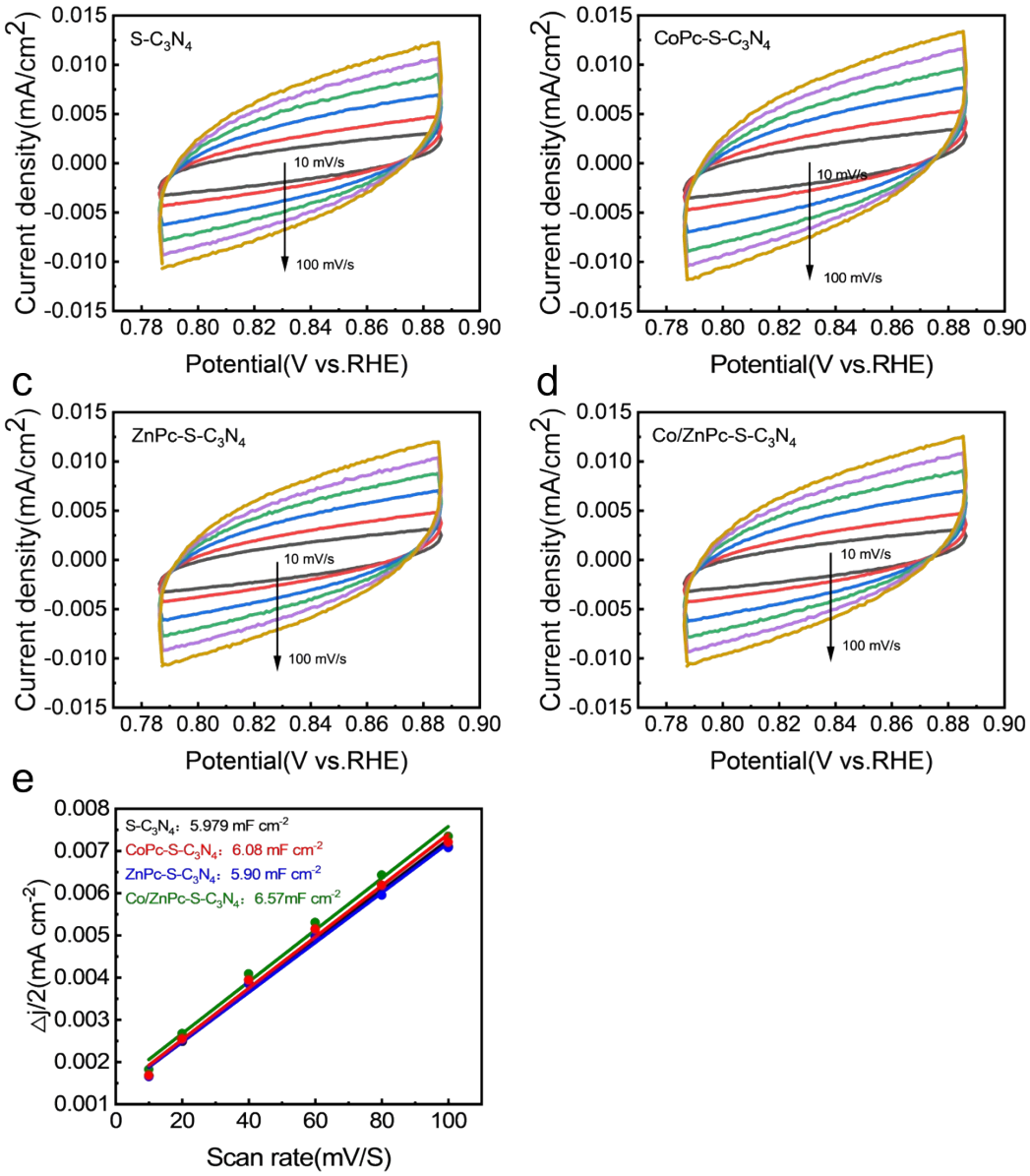

Figure S9. The ECSA was measured by double layer capacitance method. CV curves of (a) S-C_3N_4, (b) CoPc-S-C_3N_4, (c) ZnPc-S-C_3N_4 and (d) Co/ZnPc-S-C_3N_4 obtained in the capacitance region at scan rates of 10, 20, 40, 60, 80, and 100 mV/s in N_2-saturated 0.1M KOH, (e) Material corresponding double layer capacitance.

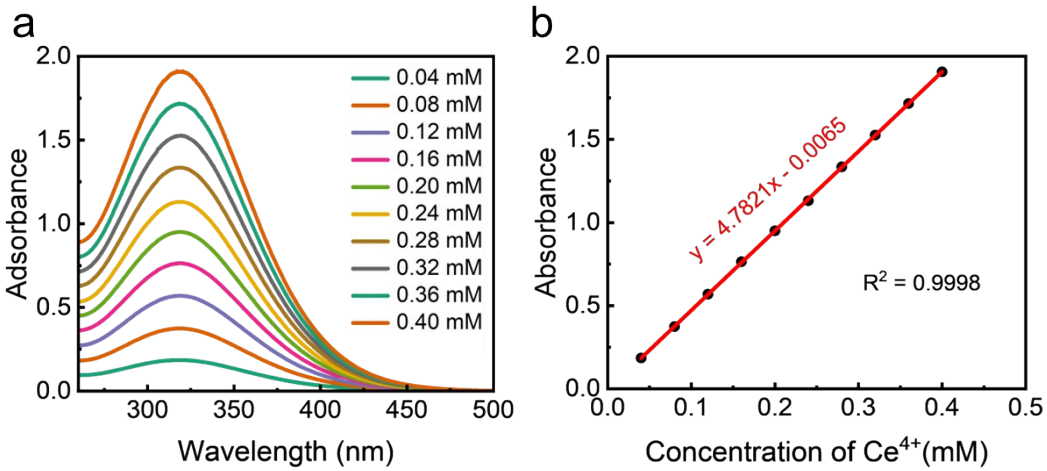

Figure S10. (a) UV-vis absorption spectra of Ce^{4+} solution with various concentrations and (b) its corresponding standard curve.

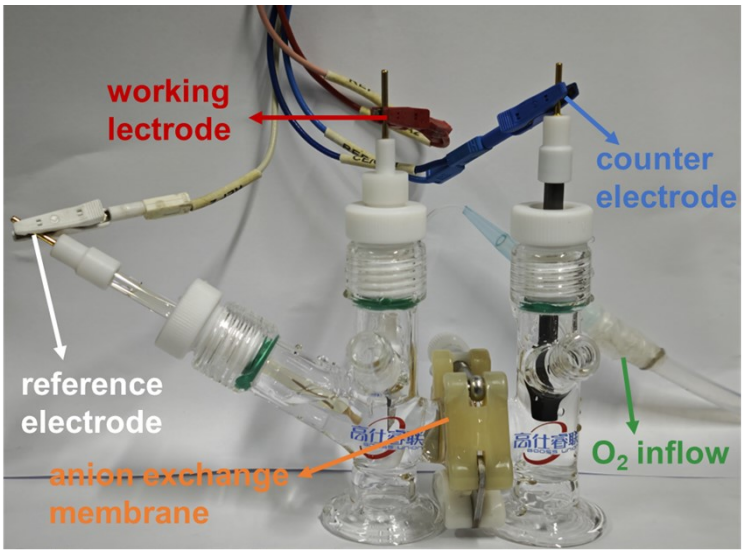

Figure S11. H-type cell installation diagram.

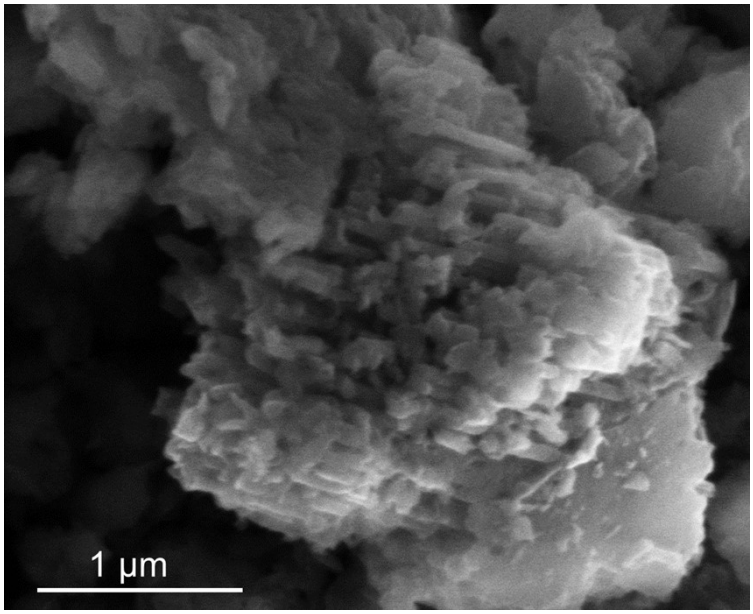

Figure S12. SEM image of Co/ZnPc-S-C_3N_4 after the stability testing.

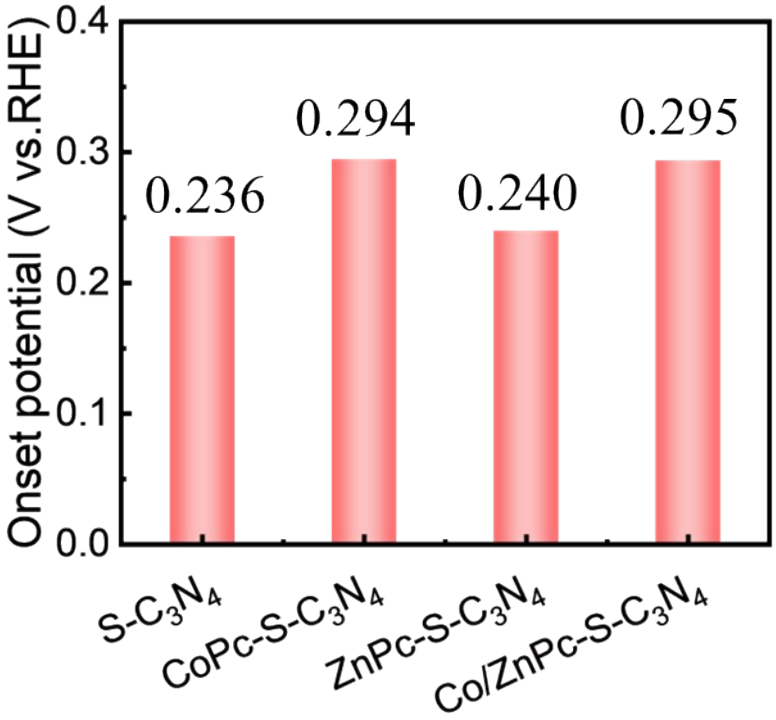

Figure S13. The onset potential at current density of 1 mA cm^{-2} at 0.1M K_2SO_4

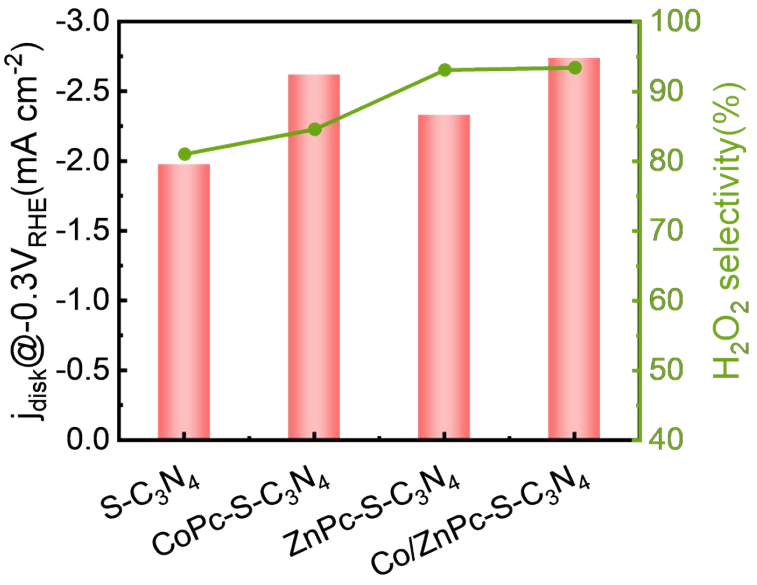

Figure S14. Relationship between current density, H_2O_2 selectivity and loaded MPc in 0.1 M K_2SO_4 electrolyte

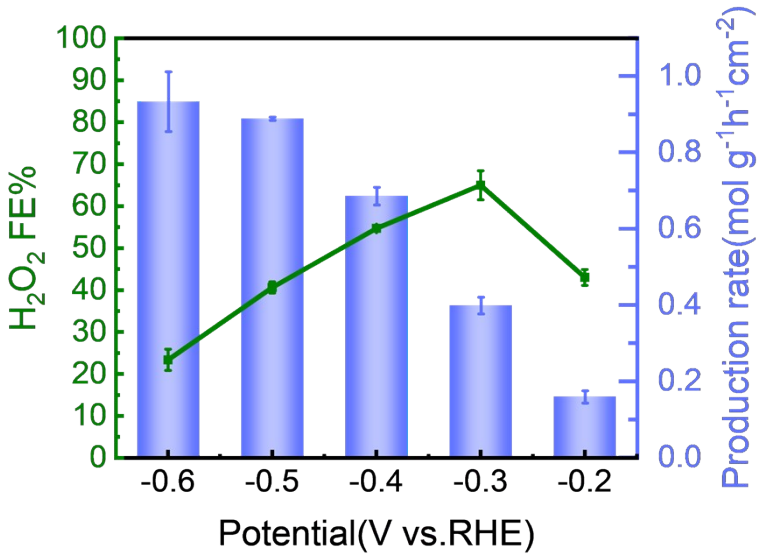

Figure S15. H_2O_2 production rate and corresponding FE of Co/ZnPc-S-C_3N_4 at different applied potentials in 0.1M $HClO_4$ electrolyte.

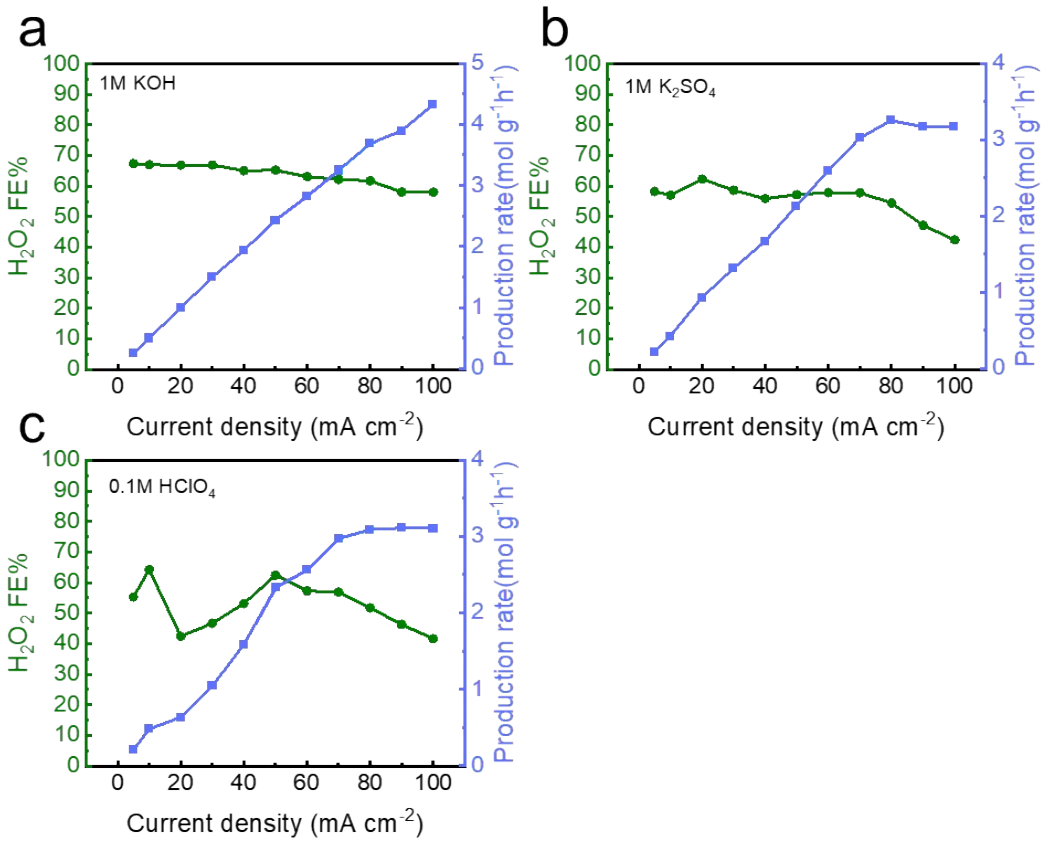

Figure S16. H_2O_2 yields and corresponding FE for Co/ZnPc-S-C_3N_4 at different current densities in (a)1M KOH, (b)1M K_2SO_4, and (c) 0.1M $HClO_4$ electrolytes.

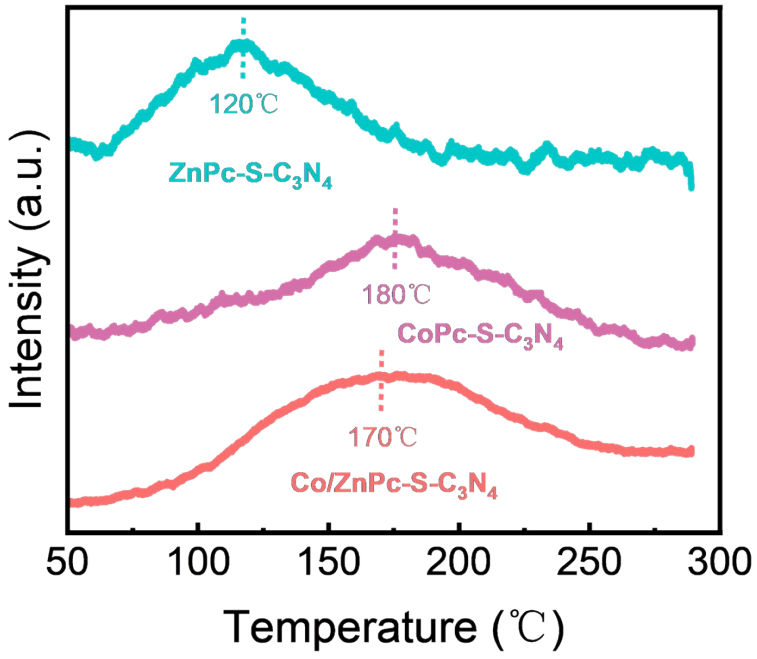

Figure S17. O_2-TPD tests for the Co/ZnPc-S-C_3N_4, CoPc-S-C_3N_4 and ZnPc-S-C_3N_4

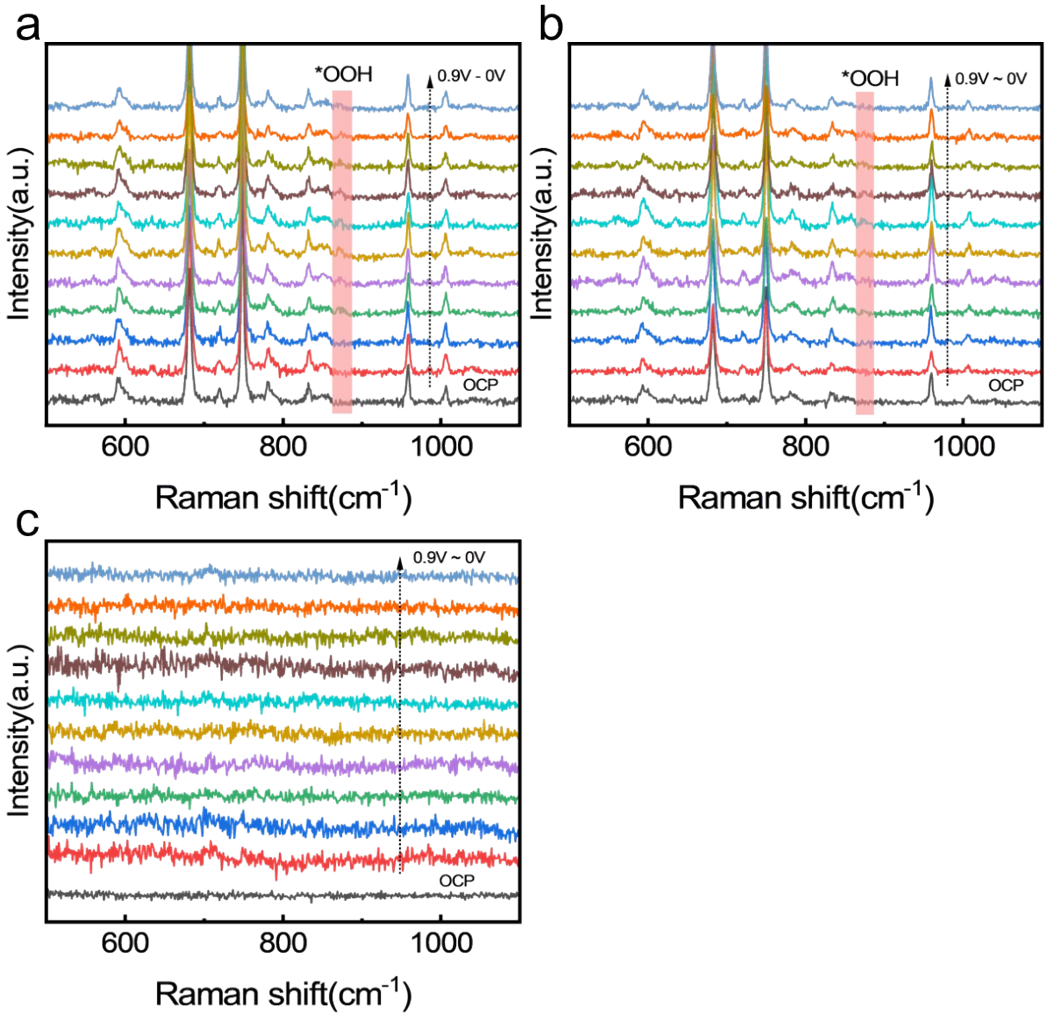

Figure S18. in situ Raman spectra of the $2e^-$ ORR on (a) Co/ZnPc-S-C_3N_4, (b) CoPc-S-C_3N_4 and (c) ZnPc-S-C_3N_4 surfaced in 0.1M KOH.

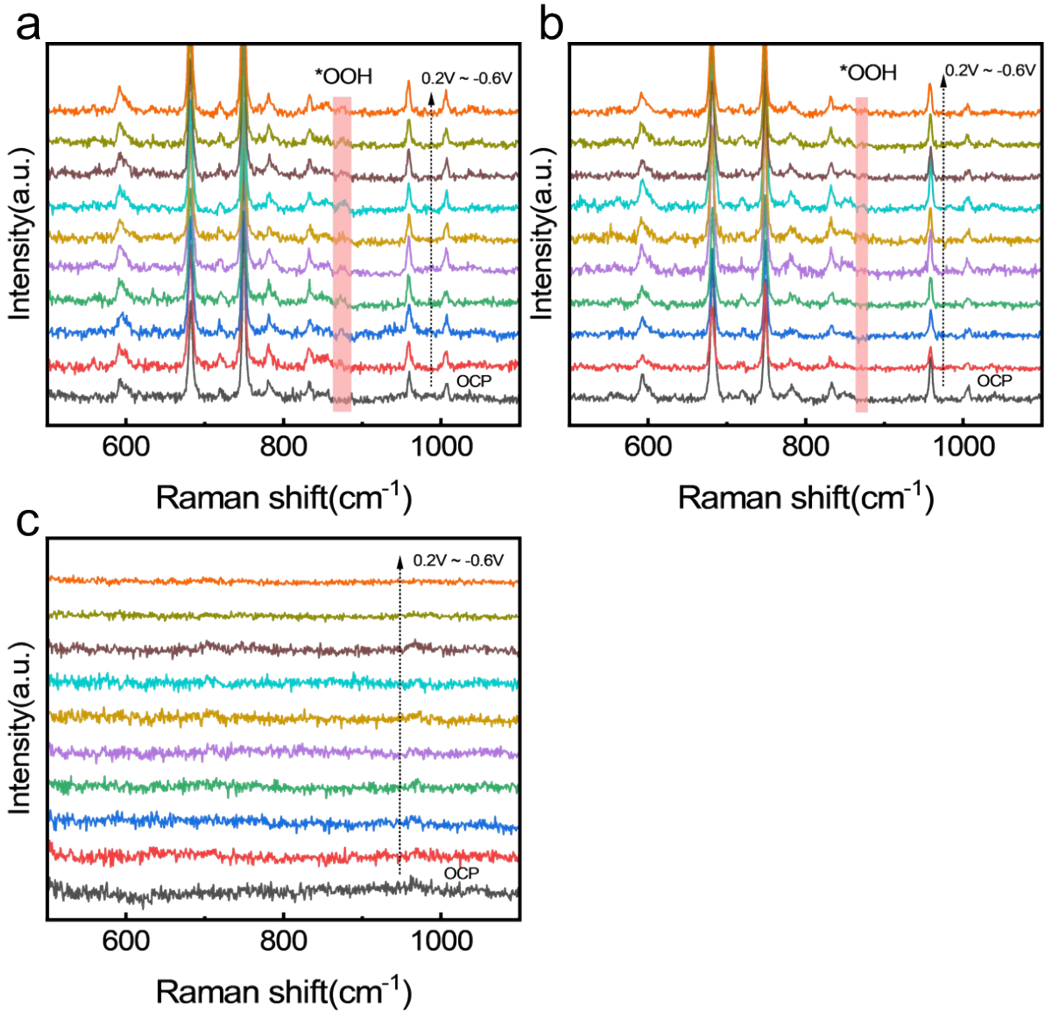

Figure S19. in situ Raman spectra of the $2e^-$ ORR on (a) Co/ZnPc-S-C_3N_4, (b) CoPc-S-C_3N_4 and (c) ZnPc-S-C_3N_4 surfaced in 0.1M K_2SO_4.

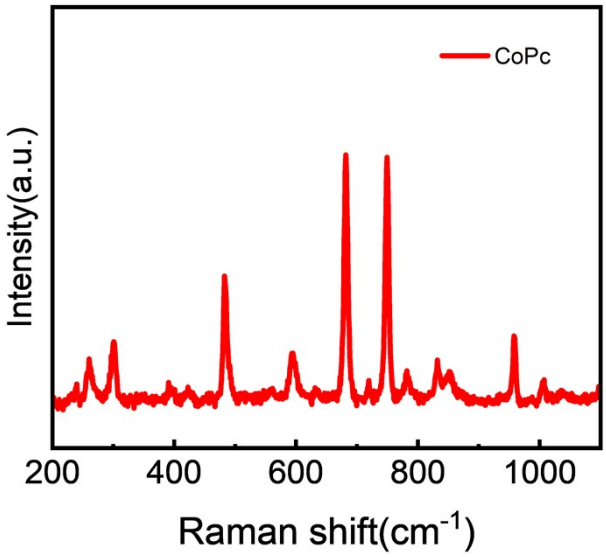

Figure S20. Raman spectrum of CoPc.

Supplementary Table S1: The EXAFS data fitting results of Co/ZnPc-S-C_3N_4.

Samples	Shell	CN [a]	R/Å [b]	σ^2/Å^2 [c]	ΔE_0/eV [d]	R-factor
Co/ZnPc-S-C_3N_4 (Co)	Co-N	4.1	1.90	0.0013	5.0	0.0132
Co/ZnPc-S-C_3N_4 (Zn)	Zn-N	4.4	2.10	0.0052	1.3	0.0096

Supplementary Table S2: The concentrations and the calculated TOF of Co and Zn in CoPc-S-C_3N_4, ZnPc-S-C_3N_4, and Co/ZnPc-S-C_3N_4 samples.

Assuming that all metal centers are active sites, the TOF was obtained at a voltage of 0.3 V vs.RHE in an alkaline medium is as follows:

	CoPc-S-C_3N_4	ZnPc-S-C_3N_4	Co/ZnPc-S-C_3N_4	
ICP	Co: 0.58%	Zn: 0.4%	Co: 0.37%	Zn: 0.2%
TOF (s^{-1})	7	6	20	40

Supplementary Table S3: Performance comparisons of Co/ZnPc-S-C_3N_4 with previously reported electrocatalysts for $2e^-$ ORR.

Sample	Electrolyte	Max H_2O_2 yield rate (mol g_{cat}^{-1} h^{-1})	Max FE (%)	Stability (h)	Cell setup	Tafel slopes mV dec^{-1}	Reference
Co/ZnPc-S-C_3N_4	**0.1M KOH**	**5.35 mol g_{cat}^{-1} h^{-1}**	**~100%**	**110**	**H-cell**	**102**	**This work**
	0.1M K_2SO_4	**5.45 mol g_{cat}^{-1} h^{-1}**	**~100%**	**85**	**H-cell**	**117**	
FeSAs/ACs-BCC	0.1 M KOH	1.13 mol g_{cat}^{-1} h^{-1}	87.8%	-	H-cell	73	[7]
$CoZn_{SA}$@CNTs	0.1M KOH	4.77 mol g_{cat}^{-1} h^{-1}	95%	12	H-cell	76.3	[8]
W1/NO-C	0.1M KOH	1.23 mol g_{cat}^{-1} h^{-1}	95%	-	H-cell	115	[9]
Ni-N_2O_2/C	0.1M KOH	1.18 mol g_{cat}^{-1} h^{-1}	97%	8	Flow cell	-	[10]
ZnCo-ZIF-C_3	0.1M KOH	4.3 mol g_{cat}^{-1} h^{-1}	95%	120	Flow cell	73.6	[11]
ZnCo-MTF	0.1M KOH	5.55 mol g_{cat}^{-1} h^{-1}	93.1%	12	Flow cell	95.4	[12]
Co-N-C	0.1M Na_2SO_4	4.33 mol g_{cat}^{-1} h^{-1}	-	8	Flow cell	-	[13]
ZnO@ZnO_2	0.1M K_2SO_4	5.47 mol g_{cat}^{-1} h^{-1}	95.5%	12	Flow cell	-	[14]
Co/NC	0.1M PBS	3.57 mol g_{cat}^{-1} h^{-1}	84.2%	10	H-cell	-	[15]
PCMNS	0.1M K_2SO_4	1.1025 mol g_{cat}^{-1} h^{-1}	-	10	H-cell	104	[16]

Reference

1. Kresse, G.; Furthmüller, J. Mater. Sci. 1996, 6, 15−50.
2. Perdew, J. P.; Burke, K.; Ernzerhof, M. Phys. Rev. Lett. 1996, 77, 3865−3868.
3. H. J. Monkhorst and J. D. Pack, *Physical Review B*, 1976, **13**, 5188-5192.
4. G. Henkelman, A. Arnaldsson and H. Jónsson, *Computational Materials Science*, 2006, **36**, 354-360.
5. E. Sanville, S. D. Kenny, R. Smith and G. Henkelman, *J Comput Chem*, 2007, **28**, 899-908.
6. M. B. Kanoun, S. Goumri-Said, U. Schwingenschlögl and A. Manchon, *Chemical Physics Letters*, 2012, **532**, 96-99.
7. H. Xu, S. Zhang, X. Zhang, M. Xu, M. Han, L. R. Zheng, Y. Zhang, G. Wang, H. Zhang and H. Zhao, *Angew Chem Int Ed Engl*, 2023, **62**, e202314414.
8. L. Yang, H. Cheng, H. Li, G. Sun, S. Liu, T. Ma and L. Zhang, *Adv Mater*, 2024, DOI: 10.1002/adma.202406957, e2406957.
9. F. Zhang, Y. Zhu, C. Tang, Y. Chen, B. Qian, Z. Hu, Y. C. Chang, C. W. Pao, Q. Lin, S. A. Kazemi, Y. Wang, L. Zhang, X. Zhang and H. Wang, *Advanced Functional Materials*, 2021, **32**.
10. Y. Wang, R. Shi, L. Shang, G. I. N. Waterhouse, J. Zhao, Q. Zhang, L. Gu and T. Zhang, *Angew Chem Int Ed Engl*, 2020, **59**, 13057-13062.
11. C. Zhang, L. Yuan, C. Liu, Z. Li, Y. Zou, X. Zhang, Y. Zhang, Z. Zhang, G. Wei and C. Yu, *J Am Chem Soc*, 2023, **145**, 7791-7799.
12. Z. M. Li, C. Q. Zhang, C. Liu, H. W. Zhang, H. Song, Z. Q. Zhang, G. F. Wei, X. J. Bao, C. Z. Yu and P. Yuan, *Angew Chem Int Ed Engl*, 2024, **63**, e202314266.
13. Y. Sun, L. Silvioli, N. R. Sahraie, W. Ju, J. Li, A. Zitolo, S. Li, A. Bagger, L. Arnarson, X. Wang, T. Moeller, D. Bernsmeier, J. Rossmeisl, F. Jaouen and P. Strasser, *J Am Chem Soc*, 2019, **141**, 12372-12381.
14. Y. Zhou, L. Xu, J. Wu, W. Zhu, T. He, H. Yang, H. Huang, T. Cheng, Y. Liu and Z. Kang, *Energy & Environmental Science*, 2023, **16**, 3526-3533.
15. H. Shen, N. Qiu, L. Yang, X. Guo, K. Zhang, T. Thomas, S. Du, Q. Zheng, J. P. Attfield, Y. Zhu and M. Yang, *Small*, 2022, **18**, e2200730.
16. R. Hu, Y. Cui, B. Huang and L. Guan, *ACS Appl Mater Interfaces*, 2021, **13**, 35856-35864.